Published in final edited form as:

Med Image Comput Comput Assist Interv. 2017 September ; 10433: 629–637. doi: 10.1007/978-3-319-66182-7_72.

Neighborhood Matching for Curved Domains with Application to Denoising in Diffusion MRI

Geng Chen[1], **Bin Dong**[2], **Yong Zhang**[3], **Dinggang Shen**[1], and **Pew-Thian Yap**[1]

[1]Department of Radiology and BRIC, University of North Carolina, Chapel Hill, USA

[2]Beijing International Center for Mathematical Research, Peking University, Beijing, China

[3]Colin Artificial Intelligence Lab, Richmond, Canada

Abstract

In this paper, we introduce a strategy for performing neighborhood matching on general non-Euclidean and non-flat domains. Essentially, this involves representing the domain as a graph and then extending the concept of convolution from regular grids to graphs. Acknowledging the fact that convolutions are features of local neighborhoods, neighborhood matching is carried out using the outcome of multiple convolutions at multiple scales. All these concepts are encapsulated in a sound mathematical framework, called graph framelet transforms (GFTs), which allows signals residing on non-flat domains to be decomposed according to multiple frequency subbands for rich characterization of signal patterns. We apply GFTs to the problem of denoising of diffusion MRI data, which can reside on domains defined in very different ways, such as on a shell, on multiple shells, or on a Cartesian grid. Our non-local formulation of the problem allows information of diffusion signal profiles of drastically different orientations to be borrowed for effective denoising.

1 Introduction

Neighborhood matching techniques such as non-local means (NLM) [1–3] cater mostly to signals defined on Cartesian grids with local neighborhoods defined via a 2D or 3D block specified by a voxel radius. However, there exist many examples of data that are not defined on regular grids. For example, the q-space sampling domains of diffusion MRI data can vary drastically, ranging from Cartesian, shell-based, to even random. It is not immediately clear how neighborhood matching techniques can be extended to these data that reside on non-Euclidean domains. Overcoming this challenge will allow neighborhood matching to be extended to data residing in curved space for applications such as data registration, interpolation, and denoising.

In this paper, we introduce a strategy for performing neighborhood matching in general curved non-Euclidean domains. This involves representing the domain as a graph, which can be seen as a representation of a manifold sampled at discrete points. We show how convolutions of functions defined on the graph can be performed, allowing different features to be computed for a local neighborhood. This will give us for each point on the domain, i.e.,

Correspondence to: Pew-Thian Yap.

each node of the graph, a feature vector that can be used for neighborhood matching. To allow for multiscale matching, we formulate the convolutions using graph framelet transforms (GFTs), as described next.

GFTs extend the concept of wavelet frames [4] for data defined on flat domains to curved, irregular, and unstructured domains [5]. The key idea of GFTs stems from the understanding of the eigenfunctions of the Laplace-Beltrami operator (graph Laplacian in the discrete setting) as Fourier basis on manifolds (graphs in the discrete setting) [5]. This allows quasi-affine systems, generated by dilations and shifts of wavelet functions, to be defined on manifolds [4]. This in turn allows painless construction of various types of tight wavelet frames on manifolds/graphs.

We apply our framework to the denoising of diffusion MRI data. Our formulation of the problem allows one to respect the structure of the data by adapting GFTs to various sampling schemes used for data acquisition in diffusion MRI. Our approach extends NLM beyond x-space to include q-space, allowing information from white matter regions with high curvature to be used more effectively for denoising without introducing artifacts. Experiments with synthetic and real data confirm the effectiveness of our method, in comparison with methods such non-local means (NLM) [2], non-local spatial-angular matching (NLSAM) [6], and x-q space non-local means (XQ-NLM) [7].

2 Approach

In what follows, we will discuss (1) How GFTs allow multi-scale convolutions, giving information associated with multiple subbands; (2) How GFT features can be used for neighborhood matching, and (3) How these concepts can be incorporated into a non-local denoising framework for noise removal in diffusion MRI.

2.1 Graph Framelet Transforms (GFTs)

We denote a graph by $\mathcal{G} := \{\mathcal{E}, \mathcal{V}, \omega\}$, where $\mathcal{V} := \{v_k \in \mathfrak{M} : k = 0, \ldots, K-1\}$ is a set of vertices representing points on a manifold $\mathfrak{M}$, $\mathcal{E} \subset \mathcal{V} \times \mathcal{V}$ is a set of edges relating the vertices, and $\omega : \mathcal{E} \to \mathbb{R}^+$ is a weight function. The associated adjacency matrix $\mathcal{A} := (\omega_{k,k'})$ is symmetric with $\omega_{k,k'} > 0$ if v_k and $v_{k'}$ are connected by an edge in $\mathcal{E}$; otherwise $\omega_{k,k'} = 0$. Given the degree matrix $D := \mathrm{diag}\{d[1], d[2], \ldots, d[K]\}$, where $d[k] := \Sigma_{k'} \omega_{k,k'}$, the graph Laplacian, defined as $\mathcal{L} := D - \mathcal{A}$, is consistent with the Laplace-Beltrami operator of the manifold.

The key idea involved in constructing wavelet frames on a graph is to view eigenvectors $\{u_k\}_{k=0}^{K-1}$ of the graph Laplacian $\mathcal{L}$ as Fourier basis on graphs and the associated eigenvalues $\{\lambda_k\}_{k=0}^{K-1}$ as frequency components [5]. One then slices the frequency spectrum in a multi-scale fashion by using a set of masks $\{\hat{a}_r(\cdot) : r = 0, \ldots, R\}$, where $\hat{a}_0(\cdot)$ acts as a low-pass filter and $\hat{a}_r(\cdot)$ with $0 < r \le R$ as band-pass or high-pass filters. More specifically, given a function f defined on the graph $\mathcal{G}$, the graph framelet analysis transform up to level L is defined as

$$\mathbf{W}f := \{W_{l,r}f : (l,r) \in \mathscr{B}_L\}, \quad (1)$$

with $\mathfrak{B}_L := \{(1, 1), (1, 2), \ldots, (1, R), (2, 1), \ldots, (L, R)\} \cup \{(L, 0)\}$ and

$$\widehat{W_{l,r}f}[k] := \begin{cases} \hat{a}_r(\gamma^{-L+1}\tilde{\lambda}_k)\hat{f}[k] & l=1, \\ \hat{a}_r(\gamma^{-L+l}\tilde{\lambda}_k)\hat{a}_0(\gamma^{-L+l-1}\tilde{\lambda}_k)\cdots\hat{a}_0(\gamma^{-L+1}\tilde{\lambda}_k)\hat{f}[k] & 2 \le l \le L, \end{cases} \quad (2)$$

where $\tilde{\lambda}_k = (\lambda_k/\lambda_{\max})\pi$ and $\gamma > 1$ is the dilation factor. Letting $\boldsymbol{\alpha} := \mathbf{W}f$ and if the masks satisfy $\sum_{r=0}^{R}|\hat{a}_r(\xi)|^2=1$, which is one of the requirements of the unitary extension principle (UEP) [5], it is easy to show that the synthesis transform $\mathbf{W}^\top\boldsymbol{\alpha}$ gives $\mathbf{W}^\top\boldsymbol{\alpha} = \mathbf{W}^\top\mathbf{W}f = If = f$. Some examples of framelet masks are shown in Table 1. Note that operator $\mathbf{W}$ can be seen as performing convolutions on functions defined on the graph [8].

In diffusion MRI, the geometric structure of the sampling domain is captured using the adjacency matrix. Based on [9], we define the adjacency matrix $\mathscr{A} := (w_{k,k'})$ by letting

$$w_{k,k'} = \exp\left\{-\frac{1-(\hat{\mathbf{q}}_k^\top\hat{\mathbf{q}}_{k'})^2}{2\alpha_p^2}\right\}\exp\left\{-\frac{(\sqrt{b_k}-\sqrt{b_{k'}})^2}{2\sigma_p^2}\right\}, \quad (3)$$

where $\mathbf{q}_k, \mathbf{q}_{k'} \in \mathbb{R}^3$ are wavevectors, $b_k = t|\mathbf{q}_k|^2$ and $b_{k'} = t|\mathbf{q}_{k'}|^2$ are the respective b-values with t being the diffusion time, and α_p and σ_p are the tuning parameters used to control the penalization of dissimilar gradient directions and diffusion weightings, respectively.

2.2 Neighborhood Matching Using GFTs

For the k-th node of the graph $\mathscr{G}$, we can define a feature vector: $\phi[k] := \{\alpha_{l,r}[k] : (l, r) \in \mathfrak{B}_L\}$. The matching weight $w_{k;l}$ between the k-th node and the l-th node is defined as

$$w_{k;l} = \frac{1}{Z_k}\exp\left\{-\frac{\|\phi[k]-\phi[l]\|_2^2}{h_{\mathrm{GFT}}^2(k)}\right\}, \quad (4)$$

where Z_k is a normalization constant to ensure that the weights sum to one and $h_{\mathrm{GFT}}(k)$ is a parameter controlling the attenuation of the exponential function.

2.3 Non-local Denoising of Diffusion MRI in *x*-*q* Space

Our method utilizes neighborhood matching in both x-space and q-space for effective denoising. For each voxel at location $\mathbf{x}_i \in \mathbb{R}^3$, the diffusion-attenuated signal measurement $S(\mathbf{x}_i, \mathbf{q}_k)$ corresponding to the wavevector $\mathbf{q}_k$ is denoised by averaging over non-local measurements that have similar q-neighborhoods. To take into account the change in spatial location and diffusion weighting, we extend (4) to become

$$w_{i,k;j,l}=\frac{1}{Z_{i,k}}\exp\left\{-\frac{\|\phi_i[k]-\phi_j[l]\|_2^2}{h_{\mathrm{GFT}}^2(i,k)}\right\}\exp\left\{-\frac{\left(\sqrt{b_k}-\sqrt{b_l}\right)^2}{h_b^2}\right\}. \quad (5)$$

Hence

$$Z_{i,k}=\sum_{(j,l)\in\mathscr{V}_{i,k}}\exp\left\{-\frac{\|\phi_i[k]-\phi_j[l]\|_2^2}{h_{\mathrm{GFT}}^2(i,k)}\right\}\exp\left\{-\frac{\left(\sqrt{b_k}-\sqrt{b_l}\right)^2}{h_b^2}\right\}, \quad (6)$$

where h_b controls the attenuation of the second exponential function and $\mathscr{V}_{i,k}$ is the search neighborhood in x-q space associated with $S(\mathbf{x}_i, \mathbf{q}_k)$, which is determined using an x-space search radius s and a q-space search angle θ. As in [2], we set

$$h_{\mathrm{GFT}}(i,k)=\sqrt{2\beta\hat{\sigma}_{i,k}^2\,|\phi_i\,[k]|}, \quad (7)$$

where β is a constant, $|\phi_i[k]|$ denotes the length of the vector $\phi_i[k]$ and $\hat{\sigma}_k^2$ is the signal standard deviation, which is computed spatial-adaptively [2]. Similarly, we set $h_b=\sqrt{2}\sigma_b$, where σ_b is a scale parameter.

We estimate the denoised signal NL(S)($\mathbf{x}_i$, $\mathbf{q}_k$) as

$$\mathrm{NLM}(S)(i,k)=\sum_{(\mathbf{x}_j,\mathbf{q}_l)\in\mathscr{V}_{i,k}} w_{i,k;j,l}[S(\mathbf{x}_j,\mathbf{q}_l)+c_{i,k;j,l}], \quad (8)$$

where $c_{i,k;j,l}$ is a variable used to compensate for differences in signal levels due to spatial intensity inhomogeneity and signal decay in q-space, which is defined as the difference between the low-pass signals at the two nodes. The low-pass signal is given by the component with the lowest frequency given by the GFT.

2.4 Adaptation to Noncentral Chi Noise

The classic NLM is designed to remove Gaussian noise and needs to be modified for the noncentral chi (NCC) noise distribution typical in acquisition using multichannel receiver coils. Based on [2,3], we define the unbiased denoised signal UNLM(S)($\mathbf{x}_i$, $\mathbf{q}_k$) as

$$\mathrm{UNLM}(S)(\mathbf{x}_i,\mathbf{q}_k)=\sqrt{\sum_{(j,l)\in\mathscr{V}_{i,k}} w_{i,k;j,l}[S(\mathbf{x}_j,\mathbf{q}_l)+c_{i,k;j,l}]^2-2N\sigma^2}, \quad (9)$$

where σ is the Gaussian noise standard deviation that can be estimated from the image background [2], N is the number of receive channels. When there is only one receive channel (i.e., $N = 1$), the noncentral chi distribution reduces to a Rician distribution.

3 Experiments

3.1 Datasets

Synthetic Data—Using phantomαs [10], a synthetic multi-shell dataset was generated for quantitative evaluation of the proposed method. The parameters used in synthetic data simulation were consistent with the real data described next: $b = 1000, 2000, 4000$ s/mm^2, 81 non-collinear gradient directions per shell, 128 × 128 voxels with 2 × 2mm^2 resolution. Four levels of 32-channel NCC noise (3%, 6%, 9%, and 12%) were added to the resulting ground truth data. The Gaussian distribution used to construct NCC noise follows the distribution $\mathcal{N}(0, \nu(p/100))$ with noise variance determined based on noise-level percentage p and maximum signal value ν [2].

Real Data—The real dataset was acquired using the same gradient directions and b-values as the synthetic dataset. A Siemens 3T TRIO MR scanner was used for data acquisition. The imaging protocol is as follows: 96×128 imaging matrix, 2 × 2 × 2 mm^3 resolution, TE=145 ms, TR=12,200 ms, 32-channel receiver coil.

3.2 Parameter Settings

For all experiments, we used the quadratic masks and set the decomposition level to $L = 20$ for rich characterization of diffusion signal profiles. The parameters used for x-q space non-local denoising were as follows:

1. Coupé et al. [2] suggested to set $s = 2$ voxels and $\beta = 1$, we followed the former, but for the latter we set $\beta = 0.1$ since we have a greater number of patch candidates by considering the joint x-q space. Based on the theory of kernel regression, reducing the bandwidth when the sample size is large reduces bias.
2. The typical value for $\left|\sqrt{b_k} - \sqrt{b_l}\right|$ is around 10 (e.g., $\sqrt{3000} - \sqrt{2000} \approx 10$). We set $\sigma_b = 10/2 = 5$.
3. Since we were using shell-sampled data in our evaluations, we set σ_p to a small value (0.1) for greater localization.
4. In our case, the minimal angular separation of the gradient directions is around 15° for each shell. We set the q-space search angle to twice of this value, i.e., $\theta = 2 \times 15° = 30°$.
5. Since the minimal angular separation is 15°, we set $\alpha_p = \sqrt{1 - \cos^2(15°)} \approx 0.26$.
6. $N = 32$ based on the imaging protocol.

We compared our method with NLM [2], NLSAM [6], and XQ-NLM [7]. Their parameters were set as suggested in [2,6,7]. We used the peak-to-signal ratio (PSNR) as the performance metric.

3.3 Results

For synthetic data, Fig. 1 indicates that the proposed method, GF-XQ-NLM, gives greater PSNR values than other denoising methods for all noise levels. The largest improvement of GF-XQ-NLM over the next best method, XQ-NLM, is 2.1 dB at 3% noise.

Regional close-up views of diffusion-weighted (DW) images, shown in Fig. 2, demonstrate the remarkable edge-preserving property of XQ-NLM and GF-XQ-NLM. The advantages of GF-XQ-NLM over XQ-NLM can be observed from the top row of Fig. 2, where GF-XQ-NLM does not over-smooth the image, unlike XQ-NLM.

For real data, Fig. 3 confirms that both XQ-NLM and GF-XQ-NLM are effective in preserving edges while removing noise. In contrast, NLSAM and NLM blur structural boundaries. The bottom two rows of Fig. 3 also demonstrate that GF-XQ-NLM is more capable in preserving edge information than XQ-NLM.

To further demonstrate the benefits of using GFTs, we investigated the influence of denoising on the fiber orientation distribution functions (ODFs). The results, shown in Fig. 4, indicate that GF-XQ-NLM reduces spurious peaks caused by noise and gives cleaner and more coherent ODFs than XQ-NLM.

4 Conclusion

In this paper, we extend neighborhood matching to curved domains using GFTs. We apply this technique to robust denoising of diffusion MRI data in a NLM framework that harnesses the multi-scale representation capability of GFTs for neighborhood matching. Comprehensive evaluations using synthetic data and real data demonstrate that the proposed method produces denoising results with greater PSNR, better preserved edges, and significantly reduced spurious fiber ODF peaks.

Acknowledgments

This work was supported in part by NIH grants (NS093842, EB022880, EB006733, EB009634, AG041721, MH100217, and AA012388) and a NSFC grant (11671022).

References

1. Buades A, Coll B, Morel JM. A review of image denoising algorithms, with a new one. Multiscale Model. Simul. 2005; 4(2):490–530.
2. Coupé P, Yger P, Prima S, Hellier P, Kervrann C, Barillot C. An optimized blockwise nonlocal means denoising filter for 3-D magnetic resonance images. IEEE Trans. on Med. Imaging. 2008; 27(4):425–441.
3. Chen G, Zhang P, Wu Y, Shen D, Yap PT. Denoising magnetic resonance images using collaborative non-local means. Neurocomputing. 2016; 177:215–227. [PubMed: 26949289]
4. Dong, B., Shen, Z. IAS Lecture Notes Series, Summer Program on The Mathematics of Image Processing. Park City Mathematics Institute; 2010. MRA-based wavelet frames and applications.
5. Dong B. Sparse representation on graphs by tight wavelet frames and applications. Appl. Comput. Harmonic Anal. 2017; 42(3):452–479.
6. St-Jean S, Coupé P, Descoteaux M. Non local spatial and angular matching: enabling higher spatial resolution diffusion MRI datasets through adaptive denoising. Med. Image Anal. 2016; 32:115–130. [PubMed: 27082655]

7. Chen, G., Wu, Y., Shen, D., Yap, P-T. XQ-NLM: denoising diffusion mri data via *x*-*q* space non-local patch matching. In: Ourselin, S.Joskowicz, L.Sabuncu, MR.Unal, G., Wells, W., editors. MICCAI 2016. LNCS. Vol. 9902. Springer; Cham: 2016. p. 587-595.

8. Henaff, M., Bruna, J., LeCun, Y. Deep convolutional networks on graph-structured data. arXiv preprint. 2015. arXiv:1506.05163

9. Yap, P-T., Dong, B., Zhang, Y., Shen, D. Tight graph framelets for sparse diffusion MRI *q*-space representation. In: Ourselin, S.Joskowicz, L.Sabuncu, MR.Unal, G., Wells, W., editors. MICCAI 2016. LNCS. Vol. 9902. Springer; Cham: 2016. p. 561-569.

10. Caruyer, E., Daducci, A., Descoteaux, M., Houde, JC., Thiran, JP., Verma, R. ISMRM. 2014. Phantomas: a flexible software library to simulate diffusion MR phantoms.

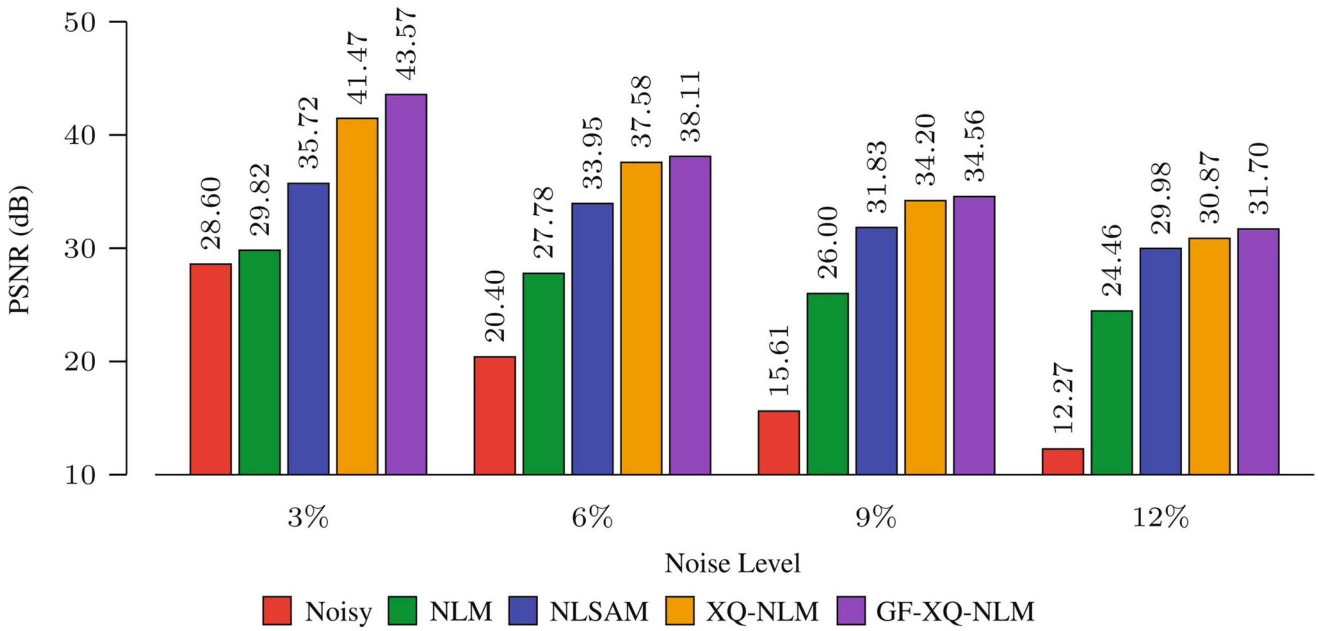

Fig. 1. PSNR Comparison

Quantitative evaluation using synthetic data.

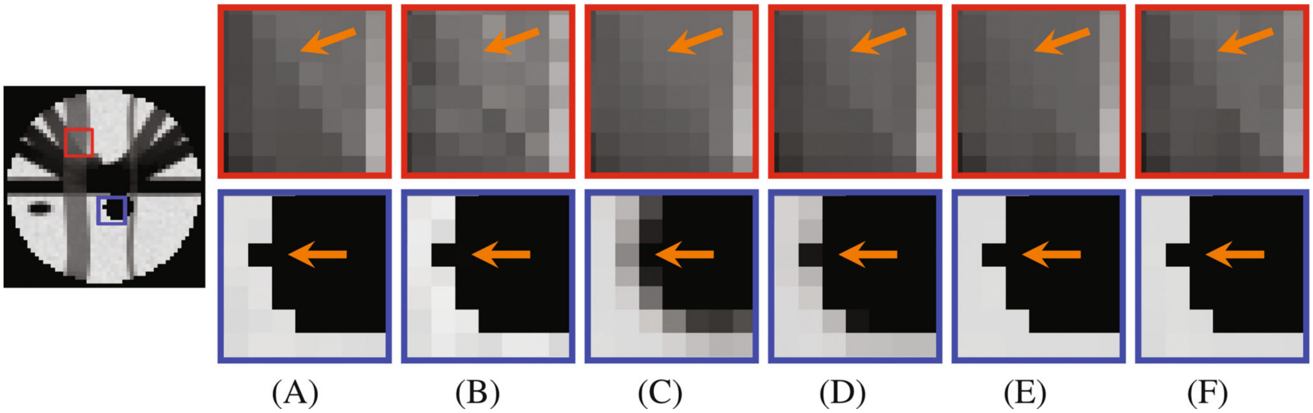

Fig. 2. DW Images – Synthetic Data

(A) Ground truth DW image. (B) DW image with 3% noise. Denoised images given by (C) NLM, (D) NLSAM, (E) XQ-NLM, and (F) GF-XQ-NLM.

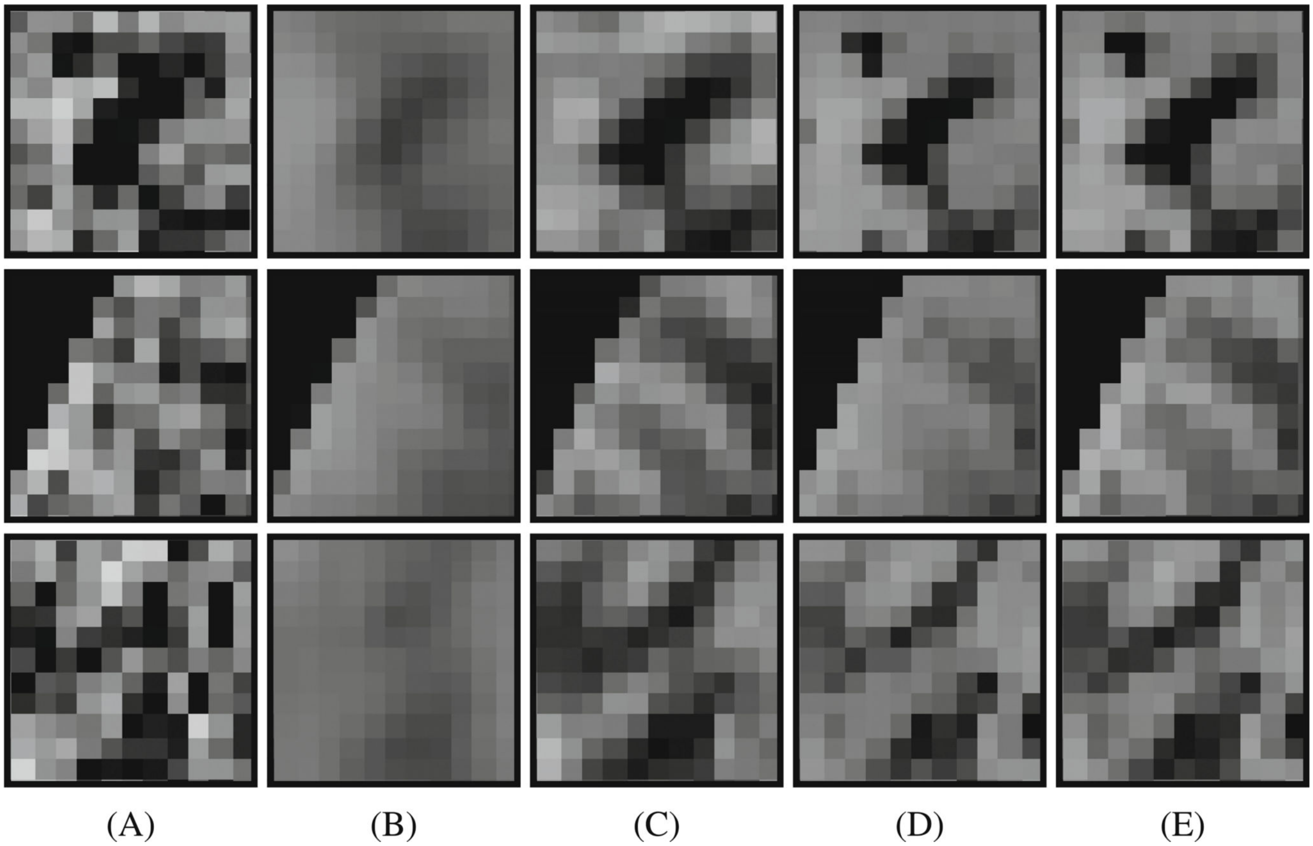

Fig. 3. DW Images – Real Data

Close-up views of (A) noisy DW image and denoised images given by (B) NLM, (C) NLSAM, (D) XQ-NLM, and (E) GF-XQ-NLM.

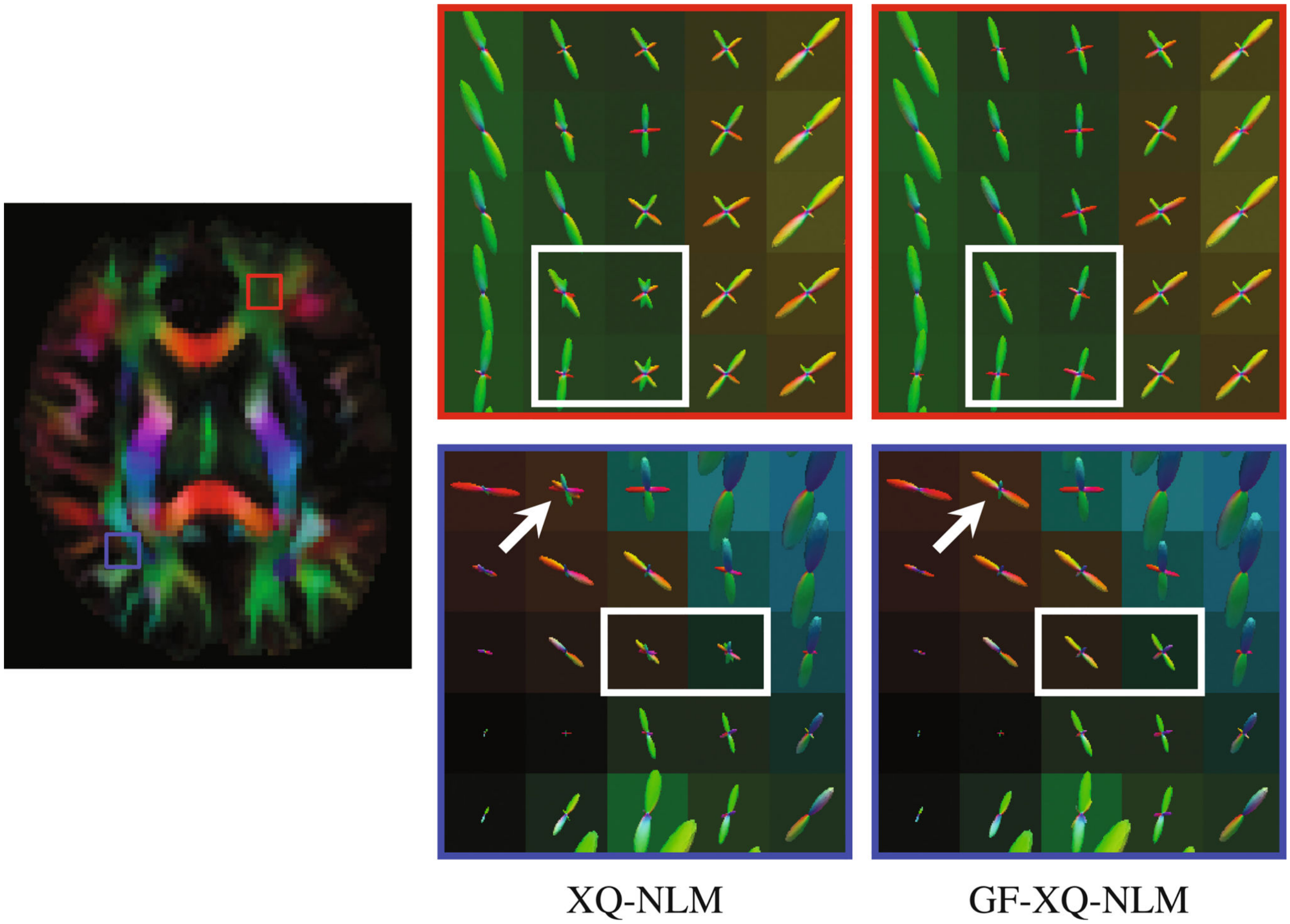

Fig. 4. Fiber ODFs

Comparison of white matter fiber ODFs given by XQ-NLM and GF-XQ-NLM.

Table 1

Framelet masks.

Haar	Linear	Quadratic
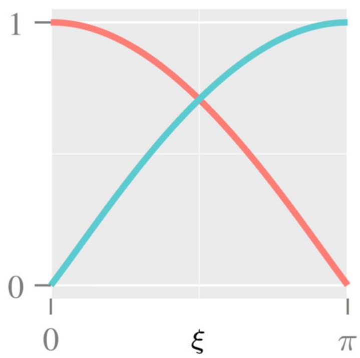	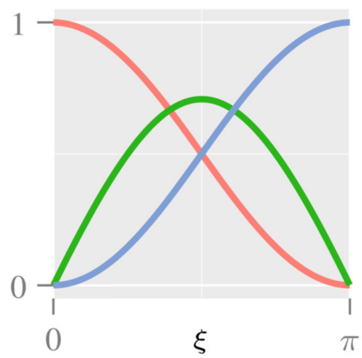	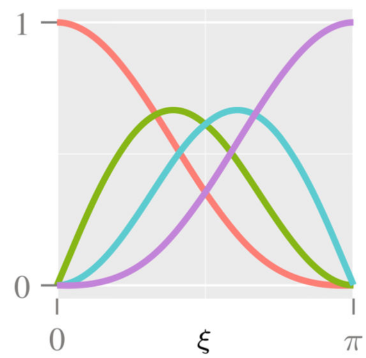
$\widehat{a}_0(\xi) = \cos(\xi/2)$ $\widehat{a}_1(\xi) = \sin(\xi/2)$	$\widehat{a}_0(\xi) = \cos^2(\xi/2)$ $\widehat{a}_1(\xi) = \frac{1}{\sqrt{2}}\sin(\xi)$ $\widehat{a}_2(\xi) = \sin^2(\xi/2)$	$\widehat{a}_0(\xi) = \cos^3(\xi/2)$ $\widehat{a}_1(\xi) = \sqrt{3}\sin(\xi/2)\cos^2(\xi/2)$ $\widehat{a}_2(\xi) = \sqrt{3}\sin^2(\xi/2)\cos(\xi/2)$ $\widehat{a}_3(\xi) = \sin^3(\xi/2)$